Structure, Vol. 12, 1425–1435, August, 2004, ©2004 Elsevier Ltd. All rights reserved. DOI 10.1016/j.str.2004.05.014

# Active Site Geometry and Substrate Recognition of the Molybdenum Hydroxylase Quinoline 2-Oxidoreductase

**Irena Bonin,[1] Berta M. Martins,[1,4] Vladimir Purvanov,[2] Susanne Fetzner,[2] Robert Huber,[1] and Holger Dobbek[3,*]**
[1]Abteilung für Strukturforschung
Max-Planck-Institut für Biochemie
82152 Martinsried
Germany
[2]Institut für Molekulare Mikrobiologie
und Biotechnologie
Westfälische Wilhelms-Universität Münster
48149 Münster
Germany
[3]Laboratorium für Proteinkristallographie
Universität Bayreuth
95440 Bayreuth
Germany

## Summary

**The soil bacterium *Pseudomonas putida* 86 uses quinoline as a sole source of carbon and energy. Quinoline 2-oxidoreductase (Qor) catalyzes the first metabolic step converting quinoline to 2-oxo-1,2-dihydroquinoline. Qor is a member of the molybdenum hydroxylases. The molybdenum ion is coordinated by two ene-dithiolate sulfur atoms, two oxo-ligands, and a catalytically crucial sulfido-ligand, whose position in the active site was controversial. The 1.8 Å resolution crystal structure of Qor indicates that the sulfido-ligand occupies the equatorial position at the molybdenum ion. The structural comparison of Qor with the allopurinol-inhibited xanthine dehydrogenase from *Rhodobacter capsulatus* allows direct insight into the mechanism of substrate recognition and the identification of putative catalytic residues. The active site protein variants QorE743V and QorE743D were analyzed to assess the catalytic role of E743.**

## Introduction

Each year approximately $15 \times 10^6$ tons of coal tars are produced worldwide, which are a source for condensed aromatics, and *N*-heteroaromatics such as quinoline (2,3-benzopyridine) (Fetzner, 1998). Under various redox conditions, microorganisms are able to metabolize naturally occurring aromatic compounds and xenobiotics. Their ability to biomineralize aromatic compounds may allow the exploitation of these microorganisms in the bioremediation of polluted areas (Fetzner, 1998). The aerobic soil bacterium *Pseudomonas putida* 86 is a chemoorganoheterotrophic organism growing on quinoline. The bacterial degradation process starts with an oxidative step catalyzed by the molybdo-iron-sulfur flavoprotein quinoline 2-oxidoreductase (Qor). Quinoline becomes hydroxylated at the C2 atom of the heterocyclic nitrogen-containing ring. The incorporated oxygen derives from water and the product of this reaction is the prevailing tautomer 2-oxo-1,2-dihydroquinoline (Scheme 1) (Bauder et al., 1990).

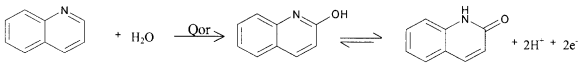


**Scheme 1: Catalytic Reaction of Qor**

Qor consists of large (L) 85 kDa, medium (M) 30 kDa, and small (S) 20 kDa subunits, which build up a dimer of heterotrimers with $(LMS)_2$ substructure. The small subunit contains two [2Fe-2S] clusters, the medium subunit is a flavoprotein with a noncovalently bound FAD cofactor, and the large subunit carries the molybdenum cofactor (Moco), which forms the active site. The Moco is a mononuclear complex of MCD (molybdopterin cytosine dinucleotide) and a molybdenum ion (Bläse et al., 1995).

Qor belongs to the molybdenum hydroxylase enzyme family (Hille, 1996). Other structurally characterized members are the aldehyde oxidoreductases from *Desulfovibrio gigas* (*dg*ALO) (Romão et al., 1995; Rebelo et al., 2001) and *D. desulfuricans* (*dd*ALO) (Rebelo et al., 2000), the carbon monoxide dehydrogenases from *Oligotropha carboxidovorans* (*oc*CODH) (Dobbek et al., 1999, 2002) and *Hydrogenophaga pseudoflava* (*hp*CODH) (Hänzelmann et al., 2000), the xanthine oxidase/dehydrogenase from *Bos taurus* milk (*bt*XO/XDH) (Enroth et al., 2000), and the xanthine dehydrogenase from *Rhodobacter capsulatus* (*rc*XDH) (Truglio et al., 2002). *Dg*ALO and *dd*ALO are functional without the flavoprotein subunit/domain usually found within this enzyme family.

Cyanide inactivation and sulfide reactivation studies of molybdenum hydroxylases (Hille, 1996) indicated the presence of a catalytically crucial active site sulfur atom whose true nature and function is the key to enzyme behavior and function (Young, 1997). The high-resolution crystal structure of *dg*ALO resulfurated at high pH with very high sulfide concentration revealed apical sulfido- and equatorial oxo- and water ligands at the active center (Huber et al., 1996). This configuration has subsequently been used to interpret the electron density of the active sites of *bt*XO/XDH (Enroth et al., 2000) and *rc*XDH (Truglio et al., 2002). In contrast to the former structures, an active site geometry with an equatorial sulfido-ligand has been identified in the true atomic resolution structure of *oc*CODH (Dobbek et al., 2002) and in the high-resolution structure of as-isolated Qor (this work). *Oc*CODH is an atypical molybdenum hydroxylase in which the sulfido-ligand bridges the two metals forming a [CuSMo(=O)OH] cluster. Qor, as well as the other characterized molybdenum hydroxylases, contains a terminal sulfido-ligand at the molybdenum ion. The position of the sulfido-ligand has direct implications for the mechanism of substrate conversion and the enigmatic functions of the sulfido- and oxo-ligands in the catalytic

*Correspondence: holger.dobbek@uni-bayreuth.de
[4]Present address: Laboratorium für Proteinkristallographie, Universität Bayreuth, 95440 Bayreuth, Germany.

cycle. Direct insight into substrate recognition and the catalytic mechanism of Qor can be gained from its comparison with *rc*XDH and *bt*XO/XDH (Truglio et al., 2002; Enroth et al., 2000) as the three enzymes catalyze the conversion of similar substrates.

Our results settle the controversy about the positioning of the sulfido-ligand in the molybdenum hydroxylase protein family. Furthermore, the structural analysis of Qor will help the design of protein variants with relevance for biotransformation.

## Results and Discussion

### Structure Determination and Quality of the Model

Qor was purified to apparent homogeneity by an ammonium sulfate fractionation followed by three chromatographic steps as previously reported (Frerichs-Deeken et al., 2003). The protein crystallized in monoclinic space group C2. The crystal structure was solved using Patterson search techniques. The complete main chains of both monomers and the vast majority of side chains, except for some surface-exposed flexible residues, were completely enveloped in the final $2F_o - F_c$ electron density map when contoured at $1\sigma$. The final model contained all residues of the protein, except the first six N-terminal amino acids of the small subunit and the three and two C-terminal amino acids of the medium and large subunits, respectively. Table 1 displays statistics for data collection, refinement, and stereochemistry deviations. Outliers in the Ramachandran plot show a well-defined electron density in both monomers.

Table 1. Statistics on Data Processing and Structure Refinement

| | |
|---|---|
| **Data Collection** | |
| Beamline | BW6/DESY |
| X-ray wavelength (Å) | 1.0500 |
| Space group | C2 |
| Unit cell parameters a, b, c (Å) | 278.32, 72.10, 202.65 |
| β (°) | 127.98 |
| Resolution (Å) | 1.80 |
| Total/unique observations | 853,819/290,508 |
| Redundancy | 2.94 |
| Completeness (%)[a] | 99.0 (99.1) |
| Mean I/σ[a,b] | 8.66 (3.56) |
| $R_{sym}$ (%)[a,c] | 7.6 (28.9) |
| **Refinement** | |
| Resolution (Å) | 20.0–1.80 |
| $R_{work}$[d] | 0.186 |
| $R_{free}$[d] | 0.207 |
| Contents per a.u. | |
| Protein molecule | 2 |
| Protein atoms | 18,482 |
| Water oxygens | 2,535 |
| Sulfate ions | 7 |
| Glycerol molecules | 9 |
| Mean B factor (Å²) | |
| Protein | 24.05 |
| Water | 38.18 |
| Sulfate | 73.76 |
| Glycerol | 47.30 |
| Rmsd[e] from ideal geometry | |
| Bond length (Å) | 0.006 |
| Bond angle (°) | 1.38 |
| Rmsd B factors (Å²) | |
| Main chain bonds | 1.04 |
| Main chain angles | 1.52 |
| Side chain bonds | 1.79 |
| Side chain angles | 2.48 |
| Ramachandran plot | |
| Most preferred | 0.903 |
| Preferred | 0.089 |
| Additional allowed | 0.007 |
| Disallowed | 0.001 |
| Cruickshanks DPI | 0.1025 |

[a] Numbers in parentheses represent statistics in the highest resolution shell (1.9–1.8 Å).
[b] Mean I/σ is the mean signal to noise ratio, where I is the intensity of the reflection and σ is the estimated error in the measurement.
[c] $R_{sym} = \Sigma_h\Sigma_i|I_{h,i} - \langle I_h\rangle|/\Sigma_h\Sigma_i\,|I_{h,i}$, where $I$ is the integrated intensity of reflection $h$ having $i$ observations and $\langle I_h\rangle$ is the mean intensity of reflection h over multiple recordings.
[d] $R_{work} = \Sigma||F_o| - |F_c||/\Sigma|F_o|$, where $F_o$ and $F_c$ are the observed and calculated structure factors. $R_{free}$ is calculated for 5% randomly chosen reflections.
[e] Rmsd, root-mean-square deviation.

### Overall Structure

Qor is a dimer in solution and two monomers were found in the asymmetric unit. The two monomers are part of two independent physiological dimers assembled by the crystallographic 2-fold axis. The dimer has overall dimensions of 149 × 111 × 78 Å³ with an accessible surface area of 77,240 Å² (Figure 1). The dimer interface is formed by a head-to-head arrangement of the two large subunits. The distance of roughly 53 Å (Figure 1) between the two molybdenum ions impairs possible cross-reaction between the two independent monomeric catalytic units. A similar arrangement of subunits has been found for all other molybdo-iron-sulfur flavoproteins displaying a butterfly-shaped dimer with two independent catalytic units.

The two monomers are basically identical with an rms deviation of 0.22 Å for $C_\alpha$ atoms. Each monomer contains three types of redox components, the Moco, the two [2Fe-2S] clusters, and the FAD. The cofactors are lined up such that the distances between them are shorter then 15 Å (Figure 1), as frequently found for redox enzymes (Page et al., 1999). The [2Fe-2S] clusters form the internal electron transfer pathway from Moco to FAD (Figure 1).

### Structure of the Three Subunits

The iron-sulfur protein or S subunit (QorS, 162 residues, yellow colored in Figure 1) is located between the M and the L subunit. QorS has dimensions of 49 × 39 × 44 Å³ and can be divided in two domains, each of them carrying one [2Fe-2S] cluster. According to EPR measurements the clusters were termed type I and type II cluster (Tshisuaka et al., 1993; Canne et al., 1997). The N-terminal domain (residues 7–82) is similar to plant-type [2Fe-2S]-cluster ferredoxins (Sticht and Rösch, 1998) and harbors the type II [2Fe-2S] cluster, which is localized next to the flavoprotein at approximately 8.3 Å to the closest atom (C7) of FAD. The C-terminal domain (residues 83–168) contains the type I [2Fe-2S] cluster, which is buried approximately 11 Å from the protein surface. The [2Fe-2S] cluster is located within the loop

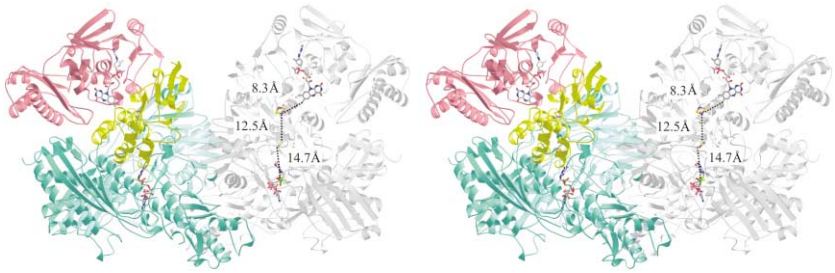


Figure 1. Structure of Qor from *Pseudomonas putida* 86

Stereo ribbon plot representation of the Qor dimer and arrangement of its cofactors. The left monomer is colored according to the subunits. The iron-sulfur containing subunit QorS is shown in yellow, the FAD-containing subunit QorM in pink and the Moco-containing subunit QorL in light blue. Cofactors are displayed as balls-and-sticks and are colored: carbon, gray; oxygen, red; nitrogen, blue; sulfur, yellow; phosphorus, magenta; iron, violet; and molybdenum, green. The right monomer is displayed in gray and rendered transparent. The shortest distances between the cofactors are shown in white boxes, starting from the molybdenum ion via the proximal type I [2Fe-2S] cluster (14.7 Å distance from the molybdenum ion to the closest iron atom) and the distal type II [2Fe-2S] cluster (12.5 Å distance between the closest iron atoms), ending at the FAD (8.3 Å distance between C7 of FAD and the nearest iron atom).

region of a four-helix bundle with 2-fold symmetry as first shown for *dg*ALO (Romão et al., 1995). The QorS structure has an additional C-terminal α helix, positioned opposite to the loop region enclosing the cluster and that runs parallel to the first helix of the bundle. The [2Fe-2S] cluster is at 14.7 Å from the molybdenum ion and at 12.5 Å from the nearest iron of the type II [2Fe-2S] cluster, thus mediating the electron transfer from the Moco to the FAD (Figure 1). The sequence of QorS is homologous to the iron-sulfur proteins of molybdenum hydroxylases with a sequence identity of 50% to *hp*CODH, 49% to *oc*CODH, 41% to *dd*ALO, 39% to *dg*ALO, 34% to *rc*XDH, and 31% to *bt*XO/XDH.

The M subunit (QorM, 285 residues, pink colored in Figure 1) is the flavoprotein of Qor with dimensions of 58 × 52 × 44 Å$^3$. QorM binds FAD and can be divided into three domains. The N-terminal domain (residues 1–53) is composed of a three-stranded parallel β sheet flanked by two α helices. This domain contains the first FAD binding motif, $^{31}$AGGQS$^{35}$, termed the glycine motif (Schulz, 1992). Although present in all members of the protein family, this binding motif is not strictly conserved. There is a single amino acid substitution (a histidine in place of glutamate) in *oc*CODH (Dobbek et al., 1999) and *hp*CODH (Hänzelmann et al., 2000), whereas *rc*XDH (Truglio et al., 2002) maintains the AGG sequence and *bt*XO/XDH (Enroth et al., 2000) has only one glycine. The middle domain (residues 59–173) is composed of a five-stranded antiparallel β sheet and six small α helices, which surround the adenosine-5′-bisphosphate-ribitol part of FAD. The second glycine motif (Schulz, 1992), $^{110}$TLGG$^{113}$ in Qor, is located in the sixth helix and is well preserved in the molybdenum hydroxylase family (TIGG in *oc*CODH, *hp*CODH and *rc*XDH, and SLGG in *bt*XO/XDH). The C-terminal domain (174–285) is formed by a three-stranded antiparallel β sheet fused with a bundle of three α helices. This domain is not involved in binding the FAD. The sequence identity of QorM to the corresponding FAD binding proteins is 33% to *oc*CODH, 30% to *hp*CODH, 23% to *rc*XDH, and 17% to *bt*XO/XDH. The residues interacting with the FAD moiety are conserved among the molybdenum hydroxylases and can be seen as fingerprints in other families of FAD binding proteins (Dobbek et al., 1999). Using the program DALI (Holm and Sander, 1993), four proteins with similar fold to QorM were identified: UDP-N-acetylmuramate dehydrogenase from *E. coli* (PDB ID code: 2MBR), cholesterol oxidase from *Brevibacterium sterolicum* (PDB ID code: 1I19), D-lactate dehydrogenase from *E. coli* (PDB ID code: 1F0X), and the vanillyl-alcohol oxidase from *Penicillium simplicissimum* (PDB ID code: 1QLT). All have been described as members of a novel family of structurally related oxidoreductases (Fraaije et al., 1998). The four proteins show a comparable architecture for the FAD binding domain and share the consensus glycine motifs ssGHs and shsG responsible for the binding of the adenosine-5′-bisphosphate part (Fraaije et al., 1998).

The isoalloxazine ring is the reactive part of FAD; it can accept two electrons and two protons or take up one proton and one hydride ion (Ghisla and Massey, 1989). In contrast to the adenosine-5′-bisphosphate-ribitol part, which is largely solvent accessible, the isoalloxazine ring is relatively well shielded within the QorM subunit, particularly by residue Y190. This residue is located in an extended loop of the C-terminal domain. Residual density indicates that the loop can move so that the carbonyl oxygen of G188 would be at hydrogen-bonding distance to the N5 nitrogen of the isoalloxazine ring resulting in the shield of the C4a and N5 atoms by Y190.

The L subunit (QorL, 786 residues, light blue in Figure 1) carries the active site with the Moco. The fold of QorL can be described as heart-like with overall dimensions of 91 × 76 × 62 Å$^3$. The subunit can be divided in two domains running almost perpendicularly to each other. The N-terminal domain (residues 1–422) interacts with both QorS and the QorM subunits and its fold is dominated by four- and five-stranded mixed β sheets. This domain is mainly responsible for anchoring the Moco and contributes to the dimer interface by interacting with the QorL subunit of the other monomer. The C-terminal domain (residues 426–786) can be further divided in two subdomains. The first (residues 426–620) is characterized by a long central α helix (residues 551–575) that runs into a three-stranded β sheet. The second (residues 620–786) consists of three β strands parallel to two α helices with a third central α helix running across the β

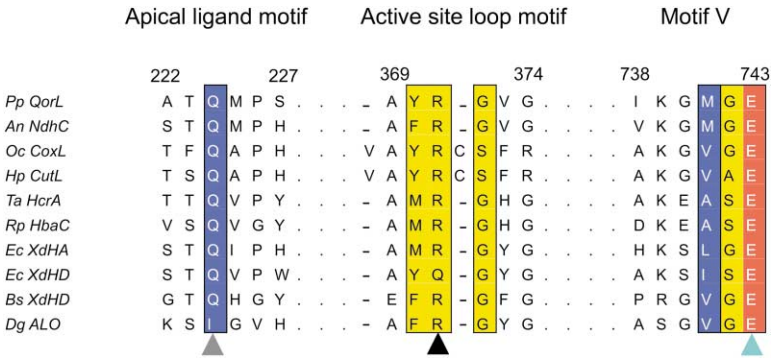


Figure 2. Phylogenetic Comparison of Molybdenum Hydroxylases

Sequence alignment of ten bacterial members of the molybdenum hydroxylase family. Numbering corresponds to the sequence of QorL. The background of identical residues is red, that of highly conserved amino acids yellow, and that of residues with similar physico-chemical properties blue. Residues (Q224, R371, and E743) involved in interactions with the Moco, belonging to the apical ligand motif, the active site loop motif, and the Motif V (Hänzelmann et al., 2000) are indicated by gray, black, and light blue arrows, respectively. Abbreviations: *Pp QorL*, *Pseudomonas putida* 86 quinoline 2-oxidoreductase large subunit; *An NdhC*, *Arthrobacter nicotinovorans* nicotine dehydrogenase; *Oc CoxL*, *Oligotropha carboxidovorans* carbon monoxide dehydrogenase large subunit; *Hp CutL*, *Hydrogenophaga pseudoflava* carbon monoxide dehydrogenase large subunit; *Ta HcrA*, *Thauera aromatica* 4-hydroxybenzoyl-CoA reductase $\alpha$ subunit; *Rp HbaC*, *Rhodopseudomonas palustris* 4-hydroxybenzoyl-CoA reductase HbaC subunit; *Ec XdHA*, *Escherichia coli* xanthine dehydrogenase, molybdenum binding subunit; *Ec XdHD*, *Escherichia coli* possible hypoxanthine oxidase xdhD; *Bs XdhD*, *Bacillus subtilis* probable xanthine dehydrogenase subunit D; *Dg ALO*, *Desulfovibrio gigas* aldehyde oxidoreductase.

strands. This subdomain creates large parts of the dimer contact. The root-mean-square distances (rmsd) for a pairwise comparison and 3D alignments of protein structures using Secondary Structure Matching (Krissinel and Henrick, 2003) have been calculated running the QorL structure against the whole PDB archive. The lowest rmsd for $C_\alpha$ atoms values were obtained for the optimal superposition to *oc*CODH and *hp*CODH structures (1.58 and 1.59 Å, respectively), followed by *dd*ALO and *dg*ALO (1.69 and 1.76 Å, respectively) and the xanthine dehydrogenases *rc*XDH and *bt*XO/XDH (1.78 and 1.97 Å, respectively). A multiple sequence alignment was performed using the protein sequence of QorL. The highest sequence similarity was with the *Arthrobacter nicotinovorans* nicotine dehydrogenase (Grether-Beck et al., 1994) followed by CODHs. QorL is less similar to *dg*ALO (Figure 2).

## The Substrate Channel

The substrate quinoline can gain access to the active site through a channel that is about 17 Å deep and 9 Å wide (distances relative to the $C_\beta$ atoms). The entrance is located at the N-terminal domain of QorL near the dimer interface and has been marked by an arrow in Figure 3. The channel is build up by residues belonging to both the N-terminal and C-terminal domains. Mostly aromatic residues (e.g., F542, F228, W331, and Y370) create a hydrophobic environment for the substrates two-ring system. Threonine residues (T90, T231, T469, T481, and T482) situated near the entrance of the channel may contribute to the substrate entrance/product release.

The channels of CODHs (Dobbek et al., 1999; Hänzelmann et al., 2000) have a diameter of 6 Å consistent with the small dimensions of the respective substrate carbon monoxide. In the case of *dg*ALO it was suggested that residues F425, F494, L497, and L626 might change their conformation to permit the different aldehyde substrates to gain access to the binding pocket (Romão et al., 1995). The structurally corresponding residues in Qor are small amino acids like A259, T332, L334, and G470 making the channel readily permeable to larger molecules like quinoline. In *rc*XDH and *bt*XO/XDH the corresponding residues are of similar size with the exception of H875 in *bt*XO/XDH (L334 in Qor). Residue G470 in Qor lies on a coil region 4.6 Å apart from the corresponding residue (phenylalanine) in *rc*XDH and *bt*XO/XDH, which results in a wider channel for Qor. TEI-6720, a potent inhibitor of *bt*XO/XDH, binds in the channel leading to the active site and it is stabilized by several conserved neutral and hydrophobic residues (Okamoto et al., 2003). The structurally corresponding residues in Qor are threonine residues with the exception of W331 (L873 in *bt*XO/XDH) and V373 (F914 in *bt*XO/XDH).

## The Qor Active Site

### *Moco and the Ligands around the Molybdenum Ion*

The Moco is composed of a molybdenum ion, which in the air-oxidized form has the oxidation state +VI and a molybdopterin cytosine dinucleotide. The ligands around the molybdenum ion can be described as having a distorted square pyramidal geometry (Figure 4A). The molybdenum ion is coordinated by two ene-dithiolate sulfurs which are positioned in the equatorial plane together with an oxo- and a sulfido-ligand. The apical ligand was modeled as an oxo-group with a distance to the molybdenum ion of 1.69 Å. Still controversial for molybdenum hydroxylases is the nature of the apical ligand. In the two crystal structures of molybdenum hydroxylases in which independent evidence could be gained for the position of the Mo-ligands (Qor and *oc*CODH), the sulfido-ligand was found in the equatorial position and an oxo-ligand was found in the apical position. In contrast, the resulfurated *dg*ALO structure (Huber et al., 1996) reveals an equatorial sulfido-ligand and an apical oxo-ligand.

To avoid model bias the three molybdenum ligands were treated from the beginning on as eight-electron atoms, corresponding to a fully occupied oxo- or a 50% occupied sulfido-ligand. Using this configuration, the B value of the refined structure indicated a clearly lower B value for one of the equatorial atoms (average $B_{SR1}$: 19.7) compared to the other two oxo-ligands ($B_{OM1}$: 26.4, $B_{OM2}$: 29.7). In addition to the lower B value positive electron density around the equatorial ligand (difference

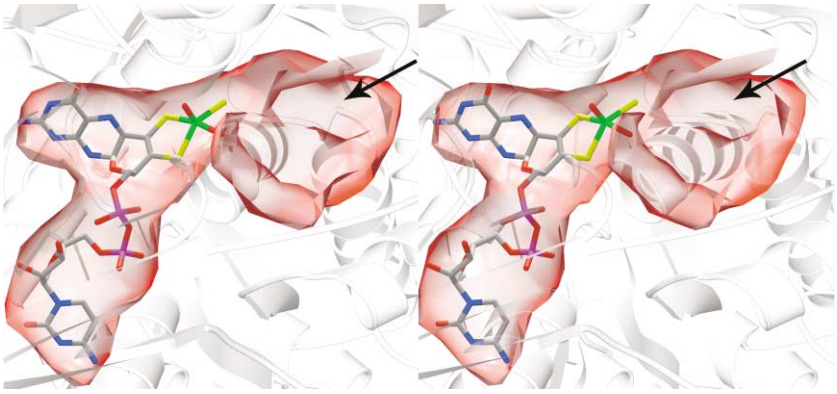

Figure 3. Stereoview of the Electrostatic Surface of the Active Site Channel

The entrance of the channel is marked by a black arrow. The channel surface was created with a probe of 1.4 Å radius. It is colored according to the electrostatic potential and rendered transparent. The side chains of residues W331 and Y545 were omitted from the calculation of the molecular surface for the purpose of a better view into the binding pocket. The Moco is shown in a ball-and-stick representation and colored like in Figure 1. The protein is represented in ribbon and rendered transparent.

Fourier map $F_o - F_c$ map at a level of 2.5$\sigma$ remained visible) indicated a lack of electrons in treating this ligand as an oxygen atom. Furthermore, the bond length of this equatorial ligand refined to 2.13 Å (average distance in the two monomers, Figure 4A), which is similar to the typical values of molybdenum sulfur double bonds of 2.18–2.19 Å (Thapper et al., 1999). After the equatorial ligand has been defined as a fully occupied sulfido-ligand the B values refined to 28.6 and no further residual density in the final difference Fourier calculations above a $\sigma$ level of 2.5 was detectable. The presence of a sulfido-ligand for Qor was identified by cyanide inactivation and

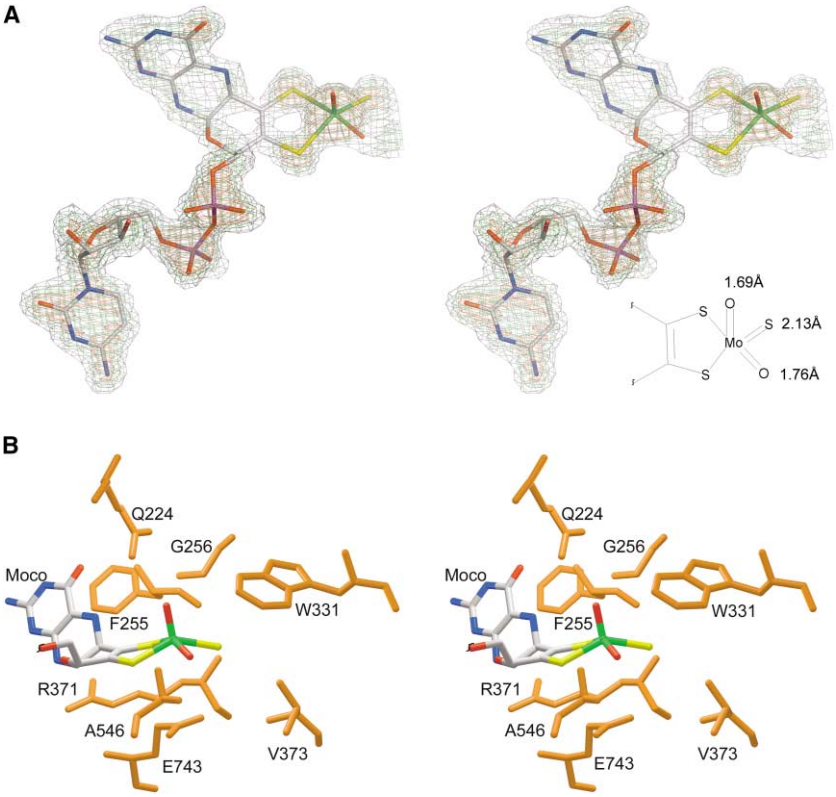


Figure 4. Stereoview of the Moco and Active Site Residues

Color code as in Figure 1.

(A) The distances from the molybdenum ion to the two oxo- and the sulfido-ligands are the average between the values observed in the two monomers. The omit $2F_o - F_c$ electron density map is contoured at 1, 2, and 3$\sigma$ (colored gray, green, and red, respectively).

(B) The Moco neighboring residues (the cytosine dinucleotide part of the Moco was removed for clarity) are colored in orange and labeled.

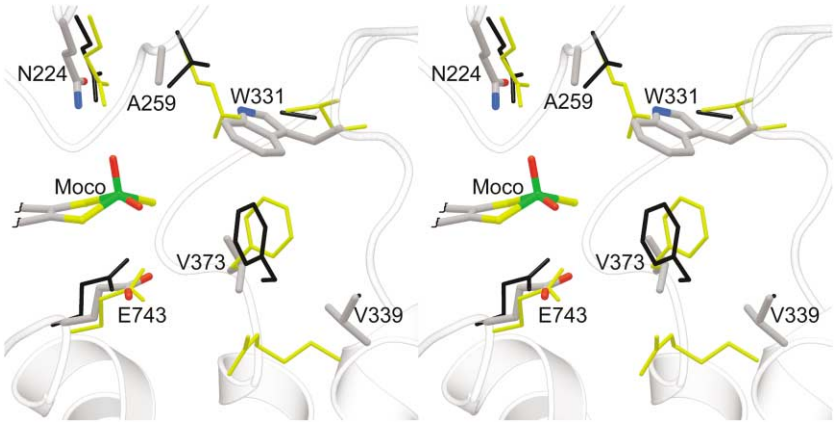


Figure 5. Stereoview of the Superposition of the Active Sites of Qor, *oc*CODH, and *rc*XDH

Residues of Qor are colored as in Figure 1, residues of *oc*CODH are colored in black, and residues of *rc*XDH in yellow. Labels correspond to Qor.

sulphide reactivation of Qor and by EPR spectroscopy of cyanide-inactivated Qor (Tshisuaka et al., 1993). New evidence in terms of a comparison between the *bt*XO/XDH and sulfite oxidase by EPR spectroscopy were recently published (Peariso et al., 2003). According to the authors, the oxo-ligand occupies the apical position in *bt*XO/XDH during the enzymatic turnover, and the large proton hyperfine coupling detected in the EPR signal in the $Mo^{V}$ state rapid type I could only be provided by a sulfhydryl proton positioned in the equatorial plane (Peariso et al., 2003). These results agree with our structural analysis of Qor and provide evidence for a conserved position of the sulfido-ligand in the family of molybdenum hydroxylases. The atypical apical position of the sulfido-ligand in *dg*ALO may be an artifact of the drastic resulfuration conditions at molar concentrations of sulfide at very high pH or it may indicate a genuine mechanistic variation of bacterial aldehyde oxidoreductases.

### *The Catalytic Pocket*

Several residues are responsible for the stabilization of the cofactor in the active site. The residues which are involved in a direct interaction with the molybdenum site (distance closer than 3.3 Å) are represented in Figure 4B. Starting from the first coordination sphere, the apical oxo-group (OM1) is at hydrogen-bonding distance to the Nϵ2 of Q224 (distance of 2.9 Å) and to the backbone nitrogen of G256 (distance of 3.1 Å), both highly conserved interactions. The equatorial oxo-ligand is at hydrogen-bonding distance to the backbone nitrogen of A546 (distance of 2.3 Å). Another highly conserved residue in Qor is F255 whose amide nitrogen is at hydrogen-bonding distance to the carbonyl atom of the pterin moiety (Figure 4B). The rings F255 and pterin are coplanar so that the pterin is stabilized by a π-π interaction. The residue E743 occupies the same position as in CODHs and *rc*XDH (Figure 5) but is further away from the molybdenum ion (distance of 4.1 Å for Qor, 3.1 Å for *oc*CODH, and 2.7 Å for *rc*XDH). The side chain of R371 adopts the same conformation in all structures with its extended side chain close to the pyrazine ring of Moco (distances of 3.7 and 3.2 Å between the guanido group and the N8 atom of the pyrazine ring). The backbone amide of R371 is at hydrogen-bonding distance to the sulfido-ligand (distance of 3.1 Å). This residue is conserved in the molybdenum hydroxylase family (black arrow in Figure 2) and is part of the active site loop $^{369}$AYR-GVG$^{374}$ of Qor. Among the molybdenum hydroxylases the consensus active site loop motif .AaR.sas (a: aromatic [F, Y, W], s: small [G, A, S], and .: all amino acids) seems to vary according to the specific substrate (Hänzelmann et al., 2000). Interestingly, the three amino acid residues Q224, R371, and E743 maintain the same conformations in all the structures with the exception of *dg*ALO/*dd*ALO, where no equivalent of the glutamine residue has been found (Figure 2).

Although not directly participating in catalysis, the apical oxo-ligand may play an important role in the stabilization of intermediate states of the catalytic cycle by increasing the Mo=O bond strength by the so-called "spectator-oxo effect" (Rappe and Goddard, 1980). The preservation of the structural environment of the molybdenum ion suggests functional importance for the residues involved. It is remarkable that only *dg*ALO and *dd*ALO lack the glutamine residue (Figures 2 and 6A). The specific role of the highly conserved glutamine (Figures 2 and 6B) appears to be the stabilization of the oxo-ligand during catalysis and biogenesis to prevent its exchange against water or a sulfido-ligand by the formation of a hydrogen bond. As *dg*ALO lacks this stabilizing interaction for the apical oxo-ligand, replacement of this ligand against a sulfido-ligand may be allowed in the presence of high concentration of sulfide.

### Putative Substrate Binding Mode

The refined structure of Qor displayed positive density in the active site of one monomer into which a glycerol molecule or a two-ring system could be modeled (Figure 7A). The presence of glycerol is not surprising since 12% of glycerol was used as a precipitating agent. The two-ring system might represent the product of the reaction (2-oxo-1,2-dihydroquinoline) or a similar compound, originating from the enzyme purification. Other crystal structures of molybdenum hydroxylases showed sub-

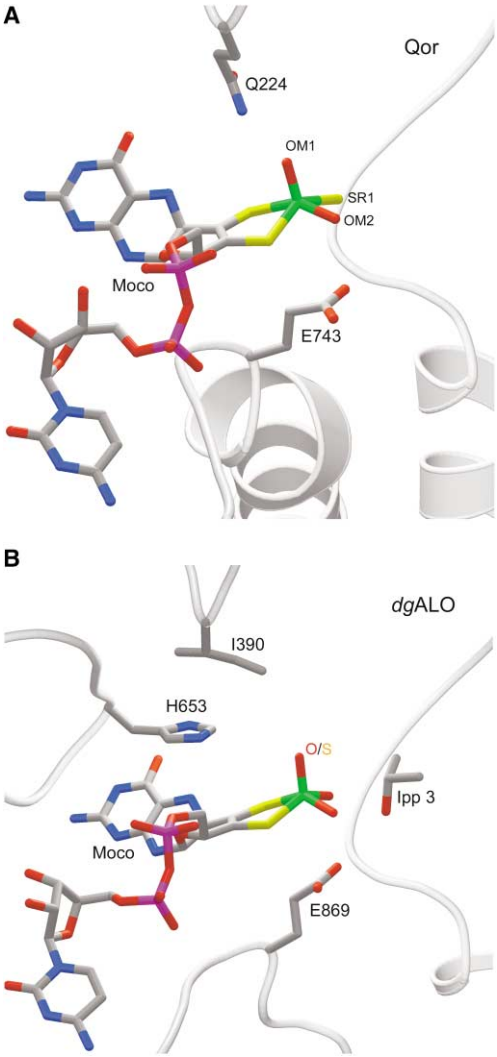


Figure 6. Comparison of the Active Sites of Qor and *dg*ALO

(A) Qor active site with the conserved Q224 at hydrogen-bonding distance to the apical oxo-ligand.

(B) *Dg*ALO active site with isopropanol (Ipp 3) in the putative substrate binding pocket. The O/S label indicates the oxo- to sulfido-substitution of the apical ligand after resulfuration (Huber et al., 1996). No stabilizing interactions are detected for the apical-ligand.

strate or product analog bound in the active site. Examples are alloxanthine in *rc*XDH (Truglio et al., 2002), salicylate in *btXO/XDH* (Enroth et al., 2000), and isopropanol in *dg*ALO (Huber et al., 1996). Alloxanthine was modeled in the active site of Qor by superposition with the *rc*XDH structure (Figure 7B). The active site pockets of the two enzymes have different hydrophilic properties. Whereas in Qor the two ligands are surrounded by V373 and W331 (Figure 7A), in *rc*XDH alloxanthine is at hydrogen-bonding distance to E232 (A259 in Qor) and R310 (V339 in Qor) (Figures 5 and 7B). From the modeled two-ring system important information can be gathered about the functional role of residues involved in substrate binding and catalytic turnover. The catalytic E743 is at 4.1 Å distance to the molybdenum ion. As seen in the case of *oc*CODH a likely role of a deprotonated glutamate is to stabilize the +VI state of the molybdenum ion (Dobbek et al., 2002). In Qor, E743 (O$\epsilon$2 atom) is at hydrogen-bonding distance to the nitrogen atom N1 of the modeled two-ring system (Figure 7A). Based on the structure, it would be reasonable that E743 contributes to substrate orientation as no other side chains are found at hydrogen-bonding distance to the N1 atom. The nucleophilic attack of the equatorial oxo-group on the C2 atom is enabled by the short distance between the two atoms (2.3 Å). Furthermore an interaction between the C2 atom and the equatorial sulfido-ligand is likely as they are 2.6 Å apart, enabling a hydride transfer between them. All other interactions with the two-ring system are of hydrophobic nature with W331 and V373 well positioned to align the aromatic two-ring system in the active site (Figures 5 and 7A). V373 is a unique feature of Qor as other structurally characterized molybdenum hydroxylases contain an aromatic residue (F/Y) at this position (Figure 5), which serves as a stacking partner for the aromatic substrate. W331 has no counterparts in the other enzymes. It is a leucine in both *bt*XO/XDH and *rc*XDH (Figure 5) and a phenylalanine in *dg*ALO. Its interaction with the two-ring system can be described as edge-on type comparable to the interaction of *bt*XO/XDH with the salicylate ring (Enroth et al., 2000).

### Active Site Protein Variants

Production of Qor proteins by *P. putida* 86-1 Δ*qor* pUF1m743a and *P. putida* 86-1 Δ*qor* pUF1m743b was verified by PAGE and Western blot analysis (data not shown). During purification, the Qor variants showed the same elution behavior in the chromatographic steps as wild-type Qor. In nondenaturating PAGE, the electrophoretic mobility of the purified Qor variants corresponded to that of the wild-type protein. Both QorE743V and QorE743D showed an about 2-fold increase in $K_{m\,app}$ (for quinoline) compared to Qor, suggesting that the replacements only slightly affect substrate affinity. In QorE743V, $k_{cat}$ was drastically reduced (Table 2), indicating the catalytic relevance of E743. In contrast, the turnover number of QorE743D was reduced only 155-fold compared to Qor, suggesting that the carboxyl group of aspartate can—to a certain extent—take over the catalytic role of the functional group of glutamate. Structurally this can be seen as an increased distance from the negative charge created by the E/D residue toward the counterpart molybdenum ion without significantly altering the provided orientation. The mutagenesis studies confirm a catalytic role for E743, since its replacement by a valine or an aspartic acid severely affects the catalytic efficiency. However, these studies do not support a crucial role of E743 in substrate binding as QorE743V shows only small changes in $K_{m\,app}$ compared to the wild-type enzyme.

### Outlook

In the present work, we unambiguously identified the equatorial position for the sulfido-ligand, which is in contrast to the previous assignment to the apical position in *dg*ALO, *bt*XO/XDH, and *rc*XDH. The currently available spectroscopical and structural data suggest that a sulfido-ligand in the equatorial position is a con-

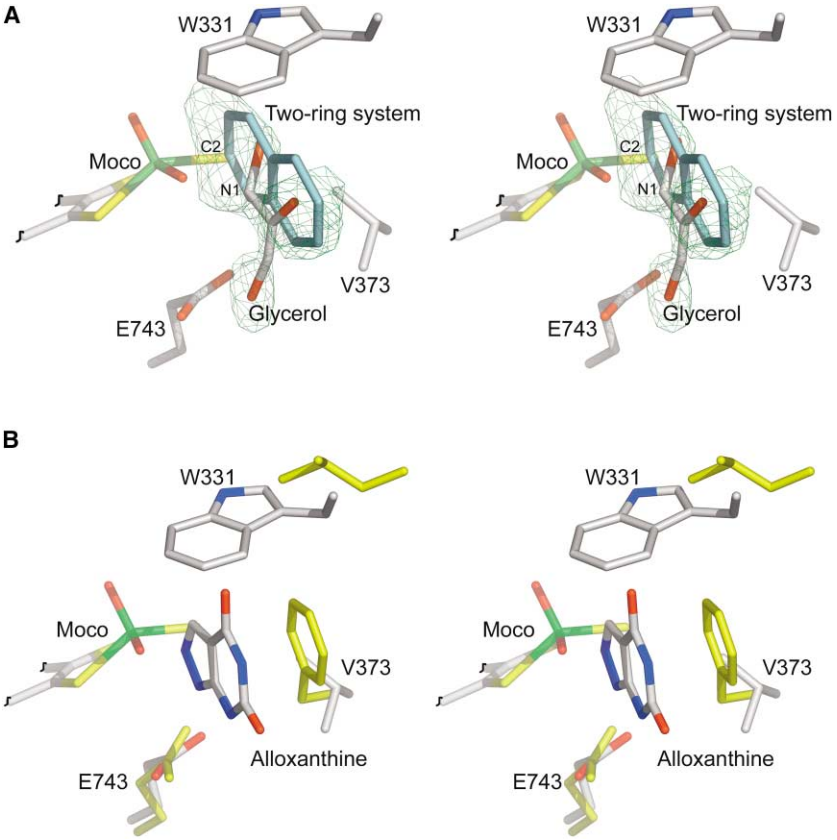


Figure 7. Stereoview of the Observed Positive Density in the Active Site of Qor

(A) The $F_o - F_c$ map contoured at 3σ is colored green. Color code for side chains and glycerol as in Figure 5. The modeled two-ring system is colored in light blue. Possible interacting residues with the two-ring system are labeled.

(B) Alloxanthine-inhibited *rc*XDH is superimposed to the Qor active site. Residues of Qor are colored as in Figure 1 and residues of *rc*XDH are colored in yellow. Alloxanthine in colored carbon, gray; oxygen, red; nitrogen, blue.

served feature in the molybdenum hydroxylase family. The results presented here provide a new structural basis toward a better understanding of the mechanism of molybdenum hydroxylases. Furthermore, studies of substrate binding and -conversion by Qor will help to predict the convertibility of other toxic organic compounds.

## Experimental Procedures

### Bacterial Strains, Plasmids, and Growth Conditions

The bacterial strains and plasmids used are listed in Table 3. *E. coli* DH5α and *Pseudomonas putida* 86-1 Δ*qor* were used as hosts for pBL9 and pUF1 derivatives, respectively. *E. coli* DH5α pBL9 clones were grown in Luria-Bertani (LB) broth containing 100 μg/ml ampicillin.

*Pseudomonas putida* 86 was cultured aerobically in 8 liter fermentors at 30°C in a quinoline minimal medium (Tshisuaka et al., 1993). When both quinoline and 2-oxo-1,2-dihydroquinoline were undetectable in the fermentation broth, further portions of 0.5 ml/l quinoline were added. *P. putida* 86-1 Δ*qor* pUF1m743a and *P. putida* 86-1 Δ*qor* pUF1m743b were grown aerobically in an 8 liter bioreactor at 30°C in mineral salts medium (Tshisuaka et al., 1993) supplemented with 1 g/l ammonium sulfate and in the presence of 500 μg/ml ampicillin. Sodium benzoate (8 mM) was added repeatedly as source of carbon and energy. It also served as XylS effector for the induction of *qorMSL* expression from the Pm promoter of the pUF1 derivatives (Frerichs-Deeken et al., 2003). As an additional XylS effector, 2-methylbenzoate was added at an optical density (600 nm) of 1, and again 4 hr before harvesting. At an optical density (600 nm) of about 4, the cells were harvested by centrifugation at 14,000 × g for 15 min at 4°C.

### Recombinant DNA Techniques

DNA restriction, dephosphorylation, ligation, and agarose gel electrophoresis were carried out using standard procedures (Sambrook et al., 1989). *E. coli* DH5α and *P. putida* 86-1 Δ*qor* were transformed

Table 2. Kinetic Parameters of Recombinant Qor and Qor Variants

| Qor Protein | $K_{m\,app}$ (Quinoline) (mM) | $k_{cat\,app}$ (Quinoline) ($s^{-1}$) |
|---|---|---|
| Qor (recombinant) | 0.12[a] | 85.4[a] |
| QorE743D | 0.25 | $5.6 \times 10^{-1}$ |
| QorE743V | 0.26 | $2.2 \times 10^{-5}$ |

[a] Frerichs-Deeken et al., 2003

Table 3. Bacterial Strains and Plasmids Used

| Strain/Plasmid | Genotype and/or Relevant Properties | Reference or Source |
|---|---|---|
| *Pseudomonas putida* 86 | Wild-type strain utilizing quinoline as sole source of carbon, nitrogen and energy | Schwarz et al., 1988 |
| *P. putida* 86-1 Δ*qor* | The two copies of *qorMSL* of *P. putida* 86-1 (Str$^r$ mutant of wild-type strain) are replaced by *npt*II and *aac*C1; Str$^r$, Kan$^r$, Gen$^r$; Qor$^-$ | Frerichs-Deeken et al., 2003 |
| *E. coli* DH5α | *supE*44 Δ*lac*U169 (ϕ 80 *lacZ*ΔM15) *hsdR*17 *recA*1 *endA*1 *gyrA*96 *thi*-1 *relA* | Hanahan, 1983 |
| pBluescript II SK(+) | colE1, *lacZ*, Ap$^r$, T3/T7 promoters | Stratagene |
| pUF1 | *qorMSL* (3786 bp PCR amplificate from *P. putida* 86 DNA) inserted into *Eco*RI-*Bam*HI sites of pJB653 (Blatny et al., 1997) | Frerichs-Deeken et al., 2003 |
| pBL9 | *Not*I-*Bam*HI fragment (2307 bp) of *qorL* cloned into pBluescript II SK(+) | this work |
| pUF1m734a | pUF1 carrying a mutation in *qorL* for the production of QorE743V | this work |
| pUF1m743b | pUF1 carrying a mutation in *qorL* for the production of QorE743D | this work |

by electroporation (Frerichs-Deeken et al., 2003). Plasmid DNA was prepared using the E.Z.N.A. Plasmid Miniprep Kit I (Peqlab, Erlangen, Germany) as specified by the supplier. For gel extraction of DNA fragments, the Nucleo Spin Extraction Kit of Macherey-Nagel (Düren, Germany) was used.

### Site-Directed Mutagenesis

Mutagenesis was performed according to the protocol of the QuikChange site-directed mutagenesis kit (Stratagene, Heidelberg, Germany). PCR was performed with pBL9 as template, using *Pfu* polymerase. The complementary mutagenic primers were as follows (the altered nucleotides are underlined: E743V, 5′-AAG GGC ATG GGC GTT TCC GCC ATG ATT TCC-3′ and 5′-AAT CAT GGC GGA AAC TCC CAT GCC CTT GAT GC-3′; E743D, 5′- AAG GGC ATG GGC GAT TCC GCC ATG ATT TCC-3′ and 5′-AAT CAT GGC GGA ATC TCC CAT GCC CTT GAT GC-3′. The pBL9 derivatives were propagated in *E. coli* DH5α, and mutations were verified by sequencing the DNA region encompassing the mutation. The *Not*I-*Bam*HI fragments of the pBL9 derivatives that carried the respective mutations were extracted from agarose gels and inserted into pUF1Δ(*Not*I-*Bam*HI), generating pUF1m743a and pUF1m743b (Table 3). Correct insertion was verified by sequencing.

### Purification of Qor and Qor Variants

Cells were suspended in 100 mM Tris-HCl buffer, pH 8.5, containing 10 μM phenylmethanesulfonylfluoride and 0.05 μl/ml Benzon nuclease (Merck, Darmstadt, Germany), and disrupted by sonification at 4°C. Cell debris was removed by centrifugation (48,000 × g, 45 min, 4°C). The supernatant was fractionated by a two-step ammonium sulfate precipitation (20% and 40% saturation, respectively), and the pellet of the 40% fraction was resuspended in buffer A (100 mM Tris-HCl [pH 8.5], 400 mM ammonium sulfate). The resulting supernatant was applied into a Phenyl Sepharose CL-4B column (Amersham-Pharmacia, Uppsala, Sweden) previously equilibrated with the buffer A (flow rate 1.5 ml/min). The column was washed with buffer B (100 mM Tris-HCl [pH 8.5], 200 mM ammonium sulfate) and a linear gradient from 0% buffer B to 100% buffer C (20 mM Tris-HCl [pH 8.5], flow rate 1.0 ml/min, 150 ml) was applied. After an isocratic flow of 75 ml of buffer C, the eluate was collected. The active pools were analyzed by native polyacrylamide gel electrophoresis and for Qor activity (see below); peak fractions were combined, concentrated (Ultrafree 50 kDa cut-off), and applied to a DEAE-Sepharose column (BioRad Laboratories, München, Germany), equilibrated with buffer D (200 mM Tris-HCl [pH 8.0]). The protein was eluted at a flow rate of 1 ml/min with a linear gradient from 300 to 900 mM Tris-HCl [pH 8.0]. Active fractions were pooled in three different batches and concentrated separately (Ultrafree 50 kDa cut-off). The concentrated protein was loaded to a Superdex G200 size exclusion column (Amersham-Pharmacia, Uppsala, Sweden) and chromatographed with 150 ml buffer E (50 mM Tris-HCl [pH 8.0], 150 mM NaCl, and flow rate 2 ml/min). Qor variants were purified as described (Frerichs-Deeken et al., 2003); however, as an additional final step, anion exchange chromatography using an UNO-Q1 column (BioRad Laboratories, München, Germany) was performed. The column was equilibrated in 50 mM Tris-HCl (pH 8.0), and the proteins were eluted using a linear gradient from the equilibration buffer to buffer containing 0.5 M NaCl. After each purification step, fractions containing Qor protein were identified by nondenaturing polyacrylamide gel electrophoresis (PAGE); gels were stained for Qor activity and/or protein. Qor preparations were concentrated to 10 mg/ml by ultrafiltration (membrane cut-off 50 kDa). Both nondenaturing and SDS-PAGE were used to check the homogeneity of the purified Qor proteins.

### Assay for Qor Activity, and Estimation of Protein Concentrations

The activity of Qor and Qor variants was determined spectrophotometrically by measuring the quinoline-dependent reduction of the artificial electron acceptor iodonitrotetrazolium chloride (INT) as described previously (Tshisuaka et al., 1993). For the kinetic analysis of QorE743V and QorE743D, quinoline concentrations were varied in the range of 0.01 to 1 mM. For the determination of apparent kinetic constants, initial velocities were fitted to the Michaelis Menten equation. Apparent $K_m$ values were deduced from Hanes plots. Protein concentrations were estimated by the method of Bradford as modified by Zor and Selinger (Zor and Selinger, 1996) using bovine serum albumin as standard protein.

### Polyacrylamide Gel Electrophoresis

SDS-PAGE (Laemmli, 1970) was performed using 12% acrylamide in the resolving gels. Nondenaturating PAGE was performed using the same protocol, but omitting the SDS in the resolving and stacking gels. Proteins were stained with Coomassie blue R-250 (0.1% [w/v] in 50% [w/v] aqueous trichloroacetic acid). For activity staining of Qor in PA gels, gels were immersed in the same buffer as used in the spectrophotometric assay, containing INT and quinoline.

### Crystallization and Data Collection

All crystallization experiments were done with the sitting drop vapor diffusion method with drop volumes between 2 and 4 μl and 500 and 1000 μl reservoirs. Crystallization conditions for Qor (10 mg/ml) were initially tested with a number of commercial and homemade incomplete factorial solutions at 20°C and 4°C. After refinement of pH and precipitant concentrations, the optimized condition was found to be 0.1 M Tris-HCl (pH 8.4), 1.4 M ammonium sulfate, 12% glycerol with protein to reservoir ratio 3:1. Crystals belonging to the space group C2 had an optimal growing time of two weeks at 4°C. The crystals could be frozen in the cooling stream (100 K; Oxford Cryosystems, Oxford, UK) after transfer into reservoir solution supplemented with 30% glycerol.

### Structure Solution and Refinement

Data to 1.80 Å resolution were collected at beamline BW6 (DESY, Hamburg) using a marCCD detector (Table 1). Indexing, integration, and reduction of the diffraction data were carried out with XDS (Kabsch, 1993). The structure was solved by Patterson search methods as implemented in AMoRe (Navazza, 1994) using a monomeric truncated poly-alanine model of *oc*CODH (PDB ID code: 1N5W). Two monomers were located in the asymmetric unit. After a rigid body and a positional refinement using CNS (Brunger et al., 1998),

density modification by 2-fold averaging was applied as implemented in RAVE (Jones, 1992). The initial $2F_o - F_c$ electron density map allowed the stepwise building of side chains in MAIN (Turk, 1996). Refinement proceeded with standard protocols (positional- and B factor refinement) in CNS (Brunger et al., 1998) and the last refinement steps were carried out without NCS restrains. PROCHECK was used for coordinate validation (Laskowski et al., 1993). The atomic coordinates have been deposited in the Protein Data Bank, www.rscb.org (PDB ID code: 1T3Q).

Figures were prepared with MOLSCRIPT (Esnouf, 1997), PyMOL (DeLano, 2002), and GRASP (Nicholls et al., 1991) and rendered using RASTER3D (Meritt and Bacon, 1997). The sequence alignment was performed using ClustalW version 1.81 (Aiyar, 2000) and displayed with ALSCRIPT (Barton, 1993).

## Acknowledgments

The authors want to acknowledge C. Breithaupt (MPI Biochemie, Germany) and G.B. Bourenkov (Desy, Germany) for synchrotron data collection. This work was supported by a European Union Grant under framework 5, European Union contract HPRN-CT-1999-00084 (to I.B. and V.P.).

Received: March 29, 2004
Revised: May 6, 2004
Accepted: May 7, 2004
Published: August 10, 2004

## References

Aiyar, A. (2000). The use of CLUSTAL W and CLUSTAL X for multiple sequence alignment. Methods Mol. Biol. *132*, 221–241.

Barton, G.J. (1993). ALSCRIPT a tool to format multiple sequence alignments. Protein Eng. *6*, 37–40.

Bauder, R., Tshisuaka, B., and Lingens, F. (1990). Quinoline oxidoreductase from *Pseudomonas putida*: a molybdenum-containing enzyme. Biol. Chem. Hoppe Seyler *371*, 1137–1144.

Bläse, M., Brunter, C., Tshisuaka, B., Fetzner, S., and Lingens, S. (1995). Cloning, expression, and sequence analysis of the three genes encoding quinoline 2-oxidoreductase, a molybdenum containing hydroxylase from *Pseudomonas putida* 86. J. Biol. Chem. *271*, 23068–23079.

Blatny, J.M., Brautaset, T., Winther-Larsen, H.C., Haugan, K., and Valla, S. (1997). Construction and use of a versatile set of broad-host-range cloning and expression vectors based on the RK2 replicon. Appl. Environ. Microbiol. *63*, 370–379.

Brunger, A.T., Adams, P.D., Clore, G.M., DeLano, W.L., Gros, P., Grosse-Kunstleve, R.W., Jiang, J.S., Kuszewski, J., Nilges, M., Pannu, N.S., et al. (1998). Crystallography & NMR system: a new software suite for macromolecular structure determination. Acta Crystallogr. D Biol. Crystallogr. *54*, 905–921.

Canne, C., Stephan, I., Finsterbusch, J., Lingens, F., Kappl, R., Fetzner, S., and Hüttermann, J. (1997). Comparative EPR and redox studies of three prokaryotic enzymes of the xanthine oxidase family: quinoline 2-oxidoreductase, quinaldine 4-oxidase and isoquinoline 1-oxidoreductase. Biochemistry *36*, 9780–9790.

DeLano, W.L. (2002). The PyMOL User's Manual (San Carlos, CA: DeLano Scientific).

Dobbek, H., Gremer, L., Meyer, O., and Huber, R. (1999). Crystal structure and mechanism of CO dehydrogenase, a molybdo iron-sulfur flavoprotein containing S-selanylcysteine. Proc. Natl. Acad. Sci. USA *96*, 8884–8889.

Dobbek, H., Gremer, L., Kiefersauer, R., Huber, R., and Meyer, O. (2002). Catalysis at a dinuclear [CuSMo(=O)OH] cluster in a CO dehydrogenase resolved at 1.1-Å resolution. Proc. Natl. Acad. Sci. USA *99*, 15971–15976.

Enroth, C., Eger, B.T., Okamoto, K., Nishino, T., Nishino, T., and Pai, E.F. (2000). Crystal structure of bovine milk xanthine dehydrogenase and xanthine oxidase: structure-based mechanism of conversion. Proc. Natl. Acad. Sci. USA *97*, 10723–10728.

Esnouf, R.M. (1997). An extensively modified version of MolScript that includes greatly enhanced coloring capabilities. J. Mol. Graph. Model. *15*, 132–134.

Fetzner, S. (1998). Bacterial degradation of pyridine, indole, quinoline, and their derivatives under different redox conditions. Appl. Microbiol. Biotechnol. *49*, 237–250.

Fraaije, M.W., van Berkel, W.J.H., Benen, J.A.E., Visser, J., and Mattevi, A. (1998). A novel oxidoreductase family sharing a conserved FAD-binding domain. Trends Biochem. Sci. *23*, 206–207.

Frerichs-Deeken, U., Goldenstedt, B., Gahl-Janßen, R., Kappl, R., Hüttermann, J., and Fetzner, S. (2003). Functional expression of the quinoline 2-oxidoreductase genes (*qorMSL*) in *Pseudomonas putida* KT2440 pUF1 and *P. putida* 86–1 Δ*qor* pUF1 and analysis of the Qor proteins. Eur. J. Biochem. *270*, 1567–1577.

Ghisla, S., and Massey, V. (1989). Mechanism of flavoprotein-catalyzed reactions. Eur. J. Biochem. *181*, 1–17.

Grether-Beck, S., Igloi, G.L., Pust, S., Schilz, E., Decker, K., and Brandsch, R. (1994). Structural analysis and molybdenum-dependent expression of the pAO1-encoded nicotine dehydrogenase genes of *Arthrobacter nicotinovorans*. Mol. Microbiol. *13*, 929–936.

Hanahan, D. (1983). Studies on transformation of *Escherichia coli* with plasmids. J. Mol. Biol. *166*, 557–580.

Hänzelmann, P., Dobbek, H., Gremer, L., Huber, R., and Meyer, O. (2000). The effect of intracellular molybdenum in *Hydrogenophaga pseudoflava* on the crystallographic structure of the seleno-molybdo-iron-sulfur flavoenzyme carbon monoxide dehydrogenase. J. Mol. Biol. *301*, 1221–1235.

Hille, R. (1996). The mononuclear molybdenum enzymes. Chem. Rev. *96*, 2757–2816.

Holm, L., and Sander, C. (1993). Protein-structure comparison by alignment of distance matrices. J. Mol. Biol. *233*, 123–128.

Huber, R., Hof, P., Duarte, R.O., Moura, J.J., Moura, I., Liu, M.Y., LeGall, J., Hille, R., Archer, M., and Romão, M.J. (1996). A structure–based catalytic mechanism for the xanthine oxidase family of molybdenum enzymes. Proc. Natl. Acad. Sci. USA *93*, 8846–8851.

Jones, T.A. (1992). A, yaap, asap, @#*? A set of averaging programs. In Molecular Replacement, E.J. Dodson, S. Gover, and W. Wolf, eds. (Warrington, UK: SERC Daresbury Laboratory), pp. 91–105.

Kabsch, W. (1993). Automatic processing of rotation diffraction data from crystals of initially unknown symmetry and cell constants. J. Appl. Crystallogr. *26*, 795–800.

Krissinel, E., and Henrick, K. (2003). Protein structure comparison in 3D based on secondary structure matching (SSM) followed by Cα alignment, scored by a new structural similarity function. In Proceedings of the Fifth International Conference on Molecular Structural Biology, A.J. Kungl and P.J. Kungl, eds. (Vienna), p. 88.

Laemmli, U. (1970). Cleavage of structural proteins during the assembly of the head of bacteriophage T4. Nature *227*, 680–685.

Laskowski, R.A., McArthur, M.W., Moss, D.S., and Thornton, J.M. (1993). PROCHECK: a program to check stereochemical quality of protein structures. J. Appl. Crystallogr. *33*, 491–497.

Meritt, E.A., and Bacon, D.J. (1997). Raster3D: photorealistic molecular graphics. Methods Enzymol. *277*, 505–524.

Navazza, J. (1994). AMoRe, an automated package for molecular replacement. Acta Crystallogr. A *50*, 157–163.

Nicholls, A., Sharp, K.A., and Honig, B. (1991). Protein folding and association: insights from the interfacial and thermodynamic properties of hydrocarbons. Proteins *11*, 281–296.

Okamoto, K., Eger, B.T., Nishino, T., Kondo, S., Pai, E.F., and Nishino, T. (2003). An extremely potent inhibitor of xanthine oxidoreductase. J. Biol. Chem. *278*, 1848–1855.

Page, C.C., Moser, C.C., Chen, X., and Dutton, P.L. (1999). Natural engineering principles of electron tunneling in biological oxidation-reduction. Nature *402*, 47–52.

Pearíso, K., Chohan, B.S., Carrano, C.J., and Kirk, M.L. (2003). Synthesis and EPR characterization of new models for the one-electron reduced molybdenum site of sulfite oxidase. Inorg. Chem. *42*, 6194–6203.

Rappe, A.K., and Goddard, W.A., III (1980). Bivalent spectator oxo bonds in metathesis and epoxidation alkenes. Nature *285*, 311–312.

Rebelo, J., Macieira, S., Dias, J.M., Huber, R., Ascenso, C.S., Rusnak, F., Moura, J.J.G., Moura, I., and Romão, M.J. (2000). Gene sequence and crystal structure of the aldehyde oxidoreductase from *Desulfovibrio desulfuricans* ATCC 27774. J. Mol. Biol. *297*, 135–146.

Rebelo, J.M., Dias, J.M., Huber, R., Moura, J.J.G., and Romão, M.J. (2001). Structure refinement of the aldehyde oxidoreductase from *Desulfovibrio gigas* (MOP) at 1.28 Å. J. Biol. Inorg. Chem. *6*, 791–800.

Romão, M.J., Archer, M., Moura, I., Moura, J.J.G., LeGall, J., Engh, R., Schneider, M., Hof, P., and Huber, R. (1995). Crystal structure of the xanthine oxidase-related aldehyde oxido-reductase from *D. gigas*. Science *270*, 1170–1176.

Sambrook, J., Fritsch, E.F. and Maniatis, T. (1989). Molecular Cloning: A Laboratory Manual, Second Edition (Cold Spring Harbor, NY: Cold Spring Harbor Laboratory Press).

Schulz, G.E. (1992). Binding of nucleotides by proteins. Curr. Opin. Struct. Biol. *2*, 61–67.

Schwarz, G., Senghas, E., Erben, A., Schäfer, B., Lingens, F., and Höke, H. (1988). Microbial metabolism of quinoline and related compounds. I. Isolation and characterization of quinoline-degrading bacteria. Syst. Appl. Microbiol. *10*, 185–190.

Sticht, H., and Rösch, P. (1998). The structure of iron-sulfur proteins. Prog. Biophys. Mol. Biol. *70*, 95–136.

Thapper, A., Donahue, J.P., Musgrave, K.B., Willer, M.W., Norlander, E., Hedman, B., Hodgson, K.O., and Holm, R.H. (1999). The unperturbed oxo-sulfido functional group *cis*-$Mo^{VI}OS$ related to that in the xanthine oxidase family of molybdoenzymes: synthesis, structural characterization, and reactivity aspects. Inorg. Chem. *38*, 4104–4114.

Truglio, J.J., Theis, K., Leimkühler, S., Rappa, R., Rajagopalan, K.V., and Kisker, C. (2002). Crystal structure of the active and alloxanthine-inhibited forms of xanthine dehydrogenase from *Rhodobacter capsulatus*. Structure *10*, 115–125.

Tshisuaka, B., Kappl, R., Hüttermann, J., and Lingens, F. (1993). Quinoline oxidoreductase from *Pseudomonas putida* 86: an improved purification procedure and electron paramagnetic resonance spectroscopy. Biochemistry *32*, 12928–12934.

Turk, D. (1996). MAIN 96: an interactive software for density modifications, model building, structure refinement and analysis. In Meeting of the International Union of Crystallography Macromolecular Computing School, P.E. Bourne, and K. Watepaugh, eds. (Bellingham, WA: International Union of Crystallography).

Young, C.G. (1997). Models for the molybdenum hydroxylases. J. Biol. Inorg. Chem. *2*, 810–816.

Zor, T., and Selinger, Z. (1996). Linearization of Bradford protein assay increases its sensitivity: theoretical and experimental studies. Anal. Biochem. *236*, 302–308.

## Accession Numbers

Coordinates have been deposited in the PDB under ID code 1T3Q.

## Note Added in Proof

While this manuscript was under review, K. Okamoto, K. Matsumoto, R. Hille, B.T. Eger, E.F. Pai, and T. Nishino [Proc. Natl. Acad. Sci. USA (2004), *101*, 7931–7936] published a 1.94 Å crystal structure of bovine xanthine oxidoreductase in complex with a slow substrate, in which they identified the sulfido-ligand in the equatorial position. This assignment is in agreement with the crystal structure of quinoline oxidoreductase presented in this manuscript and together confirm a conserved Mo-site architecture for the molybdenum hydroxylases.